Engineering NonBinary Rydberg Interactions via Phonons in an Optical Lattice

F. M. Gambetta,[1,2] W. Li,[1,2] F. Schmidt-Kaler,[3,4] and I. Lesanovsky[1,2]
[1]School of Physics and Astronomy, University of Nottingham, Nottingham NG7 2RD, United Kingdom
[2]Centre for the Mathematics and Theoretical Physics of Quantum Non-equilibrium Systems, University of Nottingham, Nottingham NG7 2RD, United Kingdom
[3]QUANTUM, Institut für Physik, Johannes Gutenberg-Universität Mainz, 55128 Mainz, Germany
[4]Helmholtz-Institut Mainz, 55128 Mainz, Germany

(Received 2 August 2019; revised manuscript received 17 December 2019; published 28 January 2020)

Coupling electronic and vibrational degrees of freedom of Rydberg atoms held in optical tweezer arrays offers a flexible mechanism for creating and controlling atom-atom interactions. We find that the state-dependent coupling between Rydberg atoms and local oscillator modes gives rise to two- and three-body interactions which are controllable through the strength of the local confinement. This approach even permits the cancellation of two-body terms such that three-body interactions become dominant. We analyze the structure of these interactions on two-dimensional bipartite lattice geometries and explore the impact of three-body interactions on system ground state on a square lattice. Focusing specifically on a system of ^{87}Rb atoms, we show that the effects of the multibody interactions can be maximized via a tailored dressed potential within a trapping frequency range of the order of a few hundred kilohertz and for temperatures corresponding to a $> 90\%$ occupation of the atomic vibrational ground state. These parameters, as well as the multibody induced timescales, are compatible with state-of-the-art arrays of optical tweezers. Our work shows a highly versatile handle for engineering multibody interactions of quantum many-body systems in most recent manifestations on Rydberg lattice quantum simulators.

DOI: 10.1103/PhysRevLett.124.043402

Introduction.—In the past years Rydberg atoms [1–3] held in optical tweezer arrays have emerged as a new platform for the implementation of quantum simulators and, potentially, also quantum computers [4–10]. One- [6], two- [11], and three-dimensional [12] arrays containing hundreds of qubits are in principle achievable and the wide tunability of Rydberg atoms grants high flexibility for the implementation of a whole host of quantum many-body spin models. The physical dynamics of these quantum simulators takes place in the electronic degrees of freedom (d.o.f.) which mimic a (fictitious) spin particle. Effective magnetic fields and interactions are achieved via light shifts effectuated by external laser fields and the electrostatic dipolar interaction between Rydberg states. Additional tuning with electric [13] and magnetic fields [14] permits the realization of exotic interactions, allowing for the study of ring-exchange Hamiltonians [15–18], frustrated-spin models [19–21], or crystallization phenomena [22–24]. Within this context, in the past decade systems with tunable two- and three-body interactions [25–29] have attracted a lot of attention since the latter are responsible for the emergence of many exotic quantum states of matter, ranging from topological phases [30,31] to spin liquids [32,33].

In this work we put forward a new mechanism for engineering nonbinary interactions in Rydberg tweezer arrays [6,9,34–43]. Here, each atom is held in place by a strong local harmonic potential. The simultaneous excitation of neighboring atoms to the Rydberg state gives rise to a mechanical force that couples the electronic d.o.f. to the local phonon modes. We show that this coupling gives rise to effective spin-spin interactions between excited atoms. Similar mechanisms in which effective interparticle interactions arise as a consequence of the coupling with an extra d.o.f. have been extensively studied in condensed matter systems. Here, well-known examples include the electron-electron interaction mediated by lattice phonons in metals [44] and the indirect spin-spin couplings [45] due to the Ruderman-Kittel-Kasuya-Yosida [46], superexchange [47], and Dzyaloshinskii-Moriya mechanisms [48]. In these cases, integrating out the extra d.o.f. typically results in two-body effective interactions between the remaining d.o.f. Crucially, in our system, since spins and phonons are coupled via pairs of Rydberg atoms, not only two-body but also three-body effective interactions arise. We analyze in depth the interplay between the various effective couplings in the case of two-dimensional bipartite lattice geometries, demonstrating that regimes dominated by three-body interactions can be achieved. Our results show that the multibody interactions arising from the electron-phonon coupling are highly tunable and can drive nontrivial phase transitions in the ground state of a Rydberg spin system. By tuning the local harmonic potentials, we show that checkerboard, striped, and clustered phases occur as well as signatures of frustration phenomena. Our work is directly relevant for recent developments on the

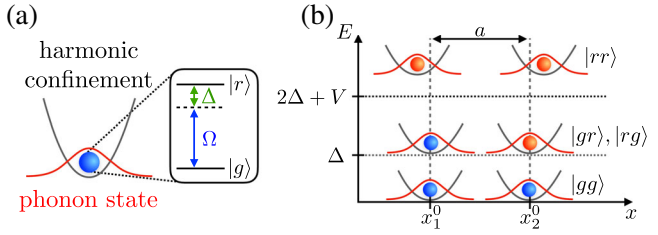

FIG. 1. Setup. (a) Each atom is modeled as a two-level system with ground state $|g\rangle$ and excited Rydberg state $|r\rangle$. The two levels are coupled by a laser with Rabi frequency Ω and detuning Δ. The atom is trapped inside a tight harmonic optical tweezer (gray) and, at low temperature, it occupies the ground state of the associated phonon d.o.f. (red). For simplicity, we assume that Rydberg and ground state experience the same trapping potential. (b) Energy diagram of a two-atom system arranged along the x axis. When both atoms are excited to the Rydberg state, $|rr\rangle$, they experience, in addition to the electronic dipolar interaction V, the potential change δV arising as a consequence of the coupling between spin and phonon d.o.f. and consisting of both two- and three-body contributions; see text for details. This also results in a state-dependent displacement $\delta x_{1,2}$ of the atoms from their equilibrium position $x^0_{1,2}$, separated by the lattice spacing a.

domain of quantum simulation with Rydberg tweezer arrays where it highlights a so far unanticipated mechanism for experimentally realizing exotic interactions.

2D model.—We consider a 2D lattice of N Rydberg atoms in the x–y plane, whose sites are labeled by $\boldsymbol{k} = (k_x, k_y)$. The electronic d.o.f. is modeled as an effective two-level system (with $|\downarrow\rangle$ and $|\uparrow\rangle$ denoting the ground state and the Rydberg excited state, respectively) [3,40]. The two levels are coupled by a laser with Rabi frequency Ω and detuning Δ [see Fig. 1(a)]. Each of the atoms, with mass m, is trapped in a strong three-dimensional harmonic potential, characterized by trapping frequencies ω_μ along the directions $\mu = x, y, z$. The atomic motion inside the confining potential can then be described in terms of the bosonic operators $b_{\boldsymbol{k},\mu}$. The Hamiltonian describing the single-particle dynamics is

$$H_{\rm sp} = \sum_{\mu=x,y,z} \sum_{\boldsymbol{k}} \hbar\omega_\mu b^\dagger_{\boldsymbol{k};\mu} b_{\boldsymbol{k};\mu} + \sum_{\boldsymbol{k}} [\Omega\sigma^x_{\boldsymbol{k}} + \Delta n_{\boldsymbol{k}}]. \quad (1)$$

Here, $n_{\boldsymbol{k}} = (1 + \sigma^z_{\boldsymbol{k}})/2$ and $\sigma^\mu_{\boldsymbol{k}}$ are the Rydberg number operator and Pauli matrices acting on the atom at site $\boldsymbol{k}$ and position $\boldsymbol{r}_k = (x_k, y_k, z_k)$, respectively. Any two atoms at lattice positions $\boldsymbol{r}_{\boldsymbol{k}}$ and $\boldsymbol{r}_{\boldsymbol{m}}$, if excited to the Rydberg state, interact through the two-body potential $V(\boldsymbol{r}_{\boldsymbol{k}}, \boldsymbol{r}_{\boldsymbol{m}})$, which depends on the interparticle distance $|\boldsymbol{r}_{\boldsymbol{k}} - \boldsymbol{r}_{\boldsymbol{m}}|$ [1,3,7]. The overall Hamiltonian is therefore $H = H_{\rm sp} + H_{\rm int}$, with

$$H_{\rm int} = {\sum_{\boldsymbol{k},\boldsymbol{m}}}' V(\boldsymbol{r}_{\boldsymbol{k}}, \boldsymbol{r}_{\boldsymbol{m}}) n_{\boldsymbol{k}} n_{\boldsymbol{m}}, \quad (2)$$

where the prime in the sum implies that terms with equal indices are excluded. Note that in Eq. (1) we have assumed the same trapping frequencies ω_μ for atoms in the ground and in the Rydberg state. This "magic" condition can be realized in Rydberg tweezer arrays through bottle beam traps [49]. Furthermore, a small frequency mismatch between the two states does not affect our central results, as discussed in the Supplemental Material (SM) [50].

At low temperature each atom oscillates around the minimum of its local potential $\boldsymbol{r}^0_{\boldsymbol{k}}$, and its position can thus be written as $\boldsymbol{r}_{\boldsymbol{k}} = \boldsymbol{r}^0_{\boldsymbol{k}} + \delta\boldsymbol{r}_{\boldsymbol{k}}$, with $\delta\boldsymbol{r}_{\boldsymbol{k};\mu} = \ell_\mu(b^\dagger_{\boldsymbol{k};\mu} + b_{\boldsymbol{k};\mu})$ being the atomic displacements from equilibrium. Here, $\boldsymbol{\ell} = (\ell_x, \ell_y, \ell_z)$ is the vector of the characteristic lengths associated with the harmonic trapping potentials in the three spatial directions with $\ell_\mu = \sqrt{\hbar(2m\omega_\mu)^{-1}}$. As a consequence, the two-body interaction depends on the displacements: $V(\boldsymbol{r}^0_{\boldsymbol{k}} + \delta\boldsymbol{r}_{\boldsymbol{k}}, \boldsymbol{r}^0_{\boldsymbol{m}} + \delta\boldsymbol{r}_{\boldsymbol{m}}) n_{\boldsymbol{k}} n_{\boldsymbol{m}}$. Clearly, this implies that a coupling between electronic and vibrational d.o.f. emerges.

This situation is reminiscent of a mechanism for creating long-range spin models in arrays of trapped ions [55–57]. In that case, the interplay of long-range Coulomb repulsion between the ions and laser induced spin-dependent forces results in an effective long-range spin-spin interaction and allows us to simulate a rich variety of quantum systems. However, in contrast to the ions, Eq. (2) implies that in our setup the potential $V(\boldsymbol{r}_{\boldsymbol{k}}, \boldsymbol{r}_{\boldsymbol{m}})$ couples electronic and vibrational d.o.f. only when two atoms are excited, which is the origin of many-body spin interaction terms.

To demonstrate this, we focus on the strong confinement regime, in which the displacements $\delta\boldsymbol{r}_{\boldsymbol{k}}$ are much smaller than interatomic distances. Indeed, this represents the typical situation in Rydberg quantum simulators [6,9,38,39]. By expanding the potential in Eq. (2) in a Taylor series to the first order in $\delta\boldsymbol{r}$, the atom-atom interaction Hamiltonian acquires the form

$$H_{\rm int} = {\sum_{\boldsymbol{k},\boldsymbol{m}}}' \left[V^0_{\boldsymbol{k},\boldsymbol{m}} + \sum_\mu W_{\boldsymbol{k},\boldsymbol{m};\mu}(b^\dagger_{\boldsymbol{k};\mu} + b_{\boldsymbol{k};\mu}) \right] n_{\boldsymbol{k}} n_{\boldsymbol{m}}, \quad (3)$$

where $V^0_{\boldsymbol{k},\boldsymbol{m}} \equiv V(\boldsymbol{r}^0_{\boldsymbol{k}}, \boldsymbol{r}^0_{\boldsymbol{m}})$ and

$$W_{\boldsymbol{k},\boldsymbol{m};\mu} = 2\ell_\mu [\nabla_{\boldsymbol{r}_{\boldsymbol{k}}} V(\boldsymbol{r}_{\boldsymbol{k}}, \boldsymbol{r}^0_{\boldsymbol{m}})|_{\boldsymbol{r}_{\boldsymbol{k}} = \boldsymbol{r}^0_{\boldsymbol{k}}}]_\mu. \quad (4)$$

Finally, since the spin-phonon coupling in Eq. (3) is linear in the bosonic operators, we can apply a polaron transformation U (see SM [50]) to decouple spin and phonon dynamics. We obtain [50,55,58]

$$UHU^\dagger = H_{\rm sp} + H_{\rm 2B} + H_{\rm 3B} + H_{\rm res} + O(\ell^2_\mu/a^2), \quad (5)$$

with

$$H_{\rm 2B} = {\sum_{\boldsymbol{k},\boldsymbol{m}}}' (V^0_{\boldsymbol{k},\boldsymbol{m}} - \tilde{V}_{\boldsymbol{k};\boldsymbol{m}}) n_{\boldsymbol{k}} n_{\boldsymbol{m}}, \quad (6a)$$

$$H_{\rm 3B} = -{\sum_{\boldsymbol{k},\boldsymbol{p},\boldsymbol{q}}}' \tilde{V}_{\boldsymbol{k};\boldsymbol{p},\boldsymbol{q}} n_{\boldsymbol{k}} n_{\boldsymbol{p}} n_{\boldsymbol{q}}. \quad (6b)$$

Here, we have introduced the coefficients $\tilde{V}_{\boldsymbol{k};\boldsymbol{p},\boldsymbol{q}} = \sum_\mu (\hbar\omega_\mu)^{-1} W_{\boldsymbol{k},\boldsymbol{p};\mu} W_{\boldsymbol{k},\boldsymbol{q};\mu}$ and $\tilde{V}_{\boldsymbol{k};\boldsymbol{m}} \equiv \tilde{V}_{\boldsymbol{k};\boldsymbol{m},\boldsymbol{m}}$. Equations (6a) and (6b) show that, as a consequence of the spin-phonon coupling, an effective atom-atom interaction emerges. The latter consists of an extra two-body [Eq. (6a)] and a novel three-body term [Eq. (6b)], whose strengths are both $\propto \tilde{V}_{\boldsymbol{k};\boldsymbol{p},\boldsymbol{q}}$. Importantly, the coefficients $\tilde{V}_{\boldsymbol{k};\boldsymbol{p},\boldsymbol{q}}$ depend on the trapping frequencies ω_μ and are therefore tunable via the harmonic confinement.

The term $H_{\rm res}$ in Eq. (5) describes a residual spin-phonon coupling, which is negligible in the limit $|W_{\boldsymbol{k},\boldsymbol{m};\mu}| \ll \hbar\omega_\mu$ [50,55,56,58]. In this regime the phonon dynamics decouples from the spins. The approximation further improves at temperatures low enough to ensure a $\gtrsim$90% population in the vibrational ground state. Such temperatures can be experimentally achieved in state-of-the-art optical tweezers via Raman sideband cooling [34,59]. Details on the validity of this spin-phonon decoupling approximation are provided in next section and in SM [50].

Microwave-dressed Rydberg states.—The strength of the phonon-mediated effective interactions in Eqs. (6a) and (6b) is directly connected to the strength of the dipolar ones: This is because the coefficients $W_{\boldsymbol{k},\boldsymbol{m};\mu}$ are proportional to the gradient of $V(\boldsymbol{r}_{\boldsymbol{k}}, \boldsymbol{r}_{\boldsymbol{m}})$. Typical dipolar interactions exhibit a power-law behavior $\propto |\boldsymbol{r}_{\boldsymbol{k}} - \boldsymbol{r}_{\boldsymbol{m}}|^{-\alpha}$ (e.g., $\alpha = 6$ for a van der Waals potential). In which case, one generally finds that $V(\boldsymbol{r}_{\boldsymbol{k}}, \boldsymbol{r}_{\boldsymbol{m}}) \gg \tilde{V}_{\boldsymbol{k};\boldsymbol{m}}$. This means that, in common situations, phonon-mediated interactions only represent a small correction. However, the interaction potential between excited atoms can be tailored via microwave (MW) dressing of two different Rydberg states [50,60,61], allowing us to make the effective interactions dominant. In Fig. 2(a) we show one possible realization of such potential, obtained via MW dressing of the atomic levels $|65S\rangle$ and $|75P\rangle$ of ^{87}Rb atoms arranged on a square lattice. Here, a and $a_{\rm NNN} = \sqrt{2}$ are the distances at equilibrium between nearest neighbors (NNs) and next-nearest neighbors (NNNs), respectively. By properly choosing the MW field parameters (see SM for details [50]), the potential can be parametrized, to a good degree of approximation, as

$$V(\boldsymbol{r}_{\boldsymbol{k}}, \boldsymbol{r}_{\boldsymbol{m}}) \approx \begin{cases} \frac{C_1}{2|\boldsymbol{r}_{\boldsymbol{k}} - \boldsymbol{r}_{\boldsymbol{m}}|^6} + \frac{c_1}{2a^6} & \text{for } |\boldsymbol{r}_{\boldsymbol{k}} - \boldsymbol{r}_{\boldsymbol{m}}| \approx a \\ \frac{C_2}{2|\boldsymbol{r}_{\boldsymbol{k}} - \boldsymbol{r}_{\boldsymbol{m}}|^6} + \frac{c_2}{2(a_{\rm NNN})^6} & \text{for } |\boldsymbol{r}_{\boldsymbol{k}} - \boldsymbol{r}_{\boldsymbol{m}}| \approx a_{\rm NNN}, \end{cases} \tag{7}$$

with, for a typical dressed potential, $V(\boldsymbol{r}_{\boldsymbol{k}}, \boldsymbol{r}_{\boldsymbol{m}}) \approx 0$ for $|\boldsymbol{r}_{\boldsymbol{k}} - \boldsymbol{r}_{\boldsymbol{m}}| > a_{\rm NNN}$ [50]. MW dressing allows us to control the values of the constants $C_{1,2}$ and $c_{1,2}$ in Eq. (7) independently and, in turn, to tune the strength of the dipolar potential (as well as its gradient) at NN and NNN distances, denoted by V_1 and V_2, respectively.

Phonon-mediated interactions.—For the case shown in Fig. 2(a), we have $V_1/\hbar \approx 0$, $V_2/\hbar \approx 2\pi \times 0.3$ MHz, and

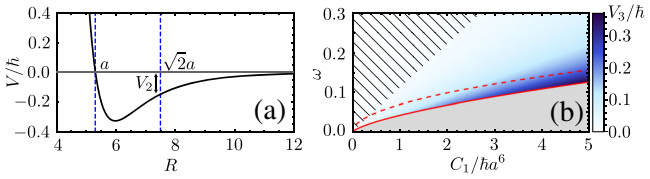

FIG. 2. MW-dressed potential and three-body interaction strength. (a) Dressed potential $V/\hbar$ (units $2\pi \times$ MHz) as a function of interatom distance R (units μm) obtained via MW dressing. See text and SM [50]. In the square lattice case, the atomic separations are $a \approx 5.3$ μm and $a_{\rm NNN} = \sqrt{2}a$ (blue dashed line). The functional form of the potential is described by Eq. (7), with $C_1/(\hbar a^6) = 2\pi \times 2.6$ MHz, $C_2/(\hbar a^6) = 2\pi \times 0.3$ MHz, $c_1 \approx -C_1$, and $c_2 = 0$. (b) Density plot of $V_3/\hbar$ as a function of $C_1/(\hbar a^6)$ and ω (units $2\pi \times$ MHz), with $\omega_\mu = \omega$. The regime with $|W_{\boldsymbol{k},\boldsymbol{m};\mu}| \leq \hbar\omega_\mu$ (in gray) is separated by the bound given in Eq. (10) (red solid curve). The case with $V_3 = V_2$ is indicated by the red dashed curve. The hatched area denotes the regime where the timescale corresponding to V_3 is > 50 μs. Here, $C_2/(\hbar a_{\rm NNN}^6) = -0.1 C_1/(\hbar a^6)$, $c_1 = -C_1$, and $c_2 = 0$.

$\hbar^{-1} dV/dR|_{R=a} = 2\pi \times 1.45$ MHz. In this way we can thus achieve regimes dominated by the phonon-mediated interactions, whose strength along the μ direction is described by the parameter

$$V_{3,\mu} = \frac{36\ell_\mu^2}{\hbar\omega_\mu a^2} \left(\frac{C_1}{a^6}\right)^2. \tag{8}$$

In this case, Eqs. (6) and (6b) become

$$H_{\rm 2B} = \sum_{\langle \boldsymbol{k},\boldsymbol{m}\rangle} (V_1 - \tilde{V}_{\boldsymbol{k};\boldsymbol{m}}) n_{\boldsymbol{k}} n_{\boldsymbol{m}} + \sum_{\langle\langle \boldsymbol{k},\boldsymbol{m}\rangle\rangle} V_2 n_{\boldsymbol{k}} n_{\boldsymbol{m}}, \tag{9a}$$

$$H_{\rm 3B} = -\sum_{\langle \boldsymbol{k},\boldsymbol{p},\boldsymbol{q}\rangle} \tilde{V}_{\boldsymbol{k};\boldsymbol{p},\boldsymbol{q}} n_{\boldsymbol{k}} n_{\boldsymbol{p}} n_{\boldsymbol{q}}, \tag{9b}$$

where, explicitly, $\tilde{V}_{\boldsymbol{k};\boldsymbol{p},\boldsymbol{q}} = V_{3,\mu} \tilde{R}^0_{\boldsymbol{k},\boldsymbol{p};\mu} \tilde{R}^0_{\boldsymbol{k},\boldsymbol{q};\mu}$, with $\tilde{\boldsymbol{R}}^0_{\boldsymbol{k},\boldsymbol{m}} = a^{-1}(\boldsymbol{r}^0_{\boldsymbol{k}} - \boldsymbol{r}^0_{\boldsymbol{m}})$. The symbols $\langle \boldsymbol{k},\boldsymbol{m}\rangle$ and $\langle\langle \boldsymbol{k},\boldsymbol{m}\rangle\rangle$ denote the sum over NNs and NNNs, respectively, while $\langle \boldsymbol{k},\boldsymbol{p},\boldsymbol{q}\rangle$ implies that the sum is restricted to sites satisfying $|\tilde{\boldsymbol{R}}^0_{\boldsymbol{k},\boldsymbol{p}}| = |\tilde{\boldsymbol{R}}^0_{\boldsymbol{k},\boldsymbol{q}}| = 1$. Note that, due to the presence of the factors $\tilde{R}^0_{\boldsymbol{k},\boldsymbol{m};\mu}$, the terms $\propto V_{3,\mu}$ strongly depend on the lattice geometry and, as we will show for the case of bipartite lattices, they give rise to anisotropic contributions in atom-atom interactions even if original dipolar forces are isotropic.

The strength of the phonon-mediated interactions can be tailored by tuning the trapping frequencies ω_μ [see Eq. (8)], which are typically of the order of hundreds of kilohertz [6,9,38,40]. In particular, Eq. (9a) implies that it is possible to make the overall two-body term vanish and maximize the effects of three-body interactions. Recalling Eq. (5), in order to decouple the electronic and vibration

d.o.f. and to focus only on the spin dynamics, we have to require $|W_{\boldsymbol{k},\boldsymbol{m};\mu}| \ll \hbar\omega_\mu$. On the other hand, to access regimes governed by the effective two- and three-body interactions, one should also consider $V_3 = \sum_\mu V_{3,\mu} \sim V_{1,2}$. From Eqs. (4) and (8), the above conditions translate into the following bounds on ω_μ:

$$\sqrt[3]{\frac{18\hbar}{ma^2}\left(\frac{C_1}{\hbar a^6}\right)^2} \ll \omega_\mu \sim \sqrt{\frac{72}{ma^2 V_{1,2}}\left(\frac{C_1}{2a^6}\right)^2}. \quad (10)$$

In Fig. 2(b), we show typical values of the effective interaction strength V_3 for a square lattice geometry. The gray region denotes the regime where $|W_{\boldsymbol{k},\boldsymbol{m};\mu}| \leq \hbar\omega_\mu$, while along the red dashed curve, $V_3 = V_2$. As discussed in more detail in SM [50], the leftmost condition in Eq. (10), which holds for any value of Ω, can be relaxed in the strong (effective) interaction regime, where $V_3/\Omega \gg |W_{\boldsymbol{k},\boldsymbol{m};\mu}|/(\hbar\omega_\mu)$, while the spin-phonon decoupling becomes exact in the classical limit (i.e., with vanishing Rabi frequency Ω). Thus, as can be seen in Fig. 2(b), the regime with $V_2 \sim V_3$ can be accessed experimentally and corresponds to trapping frequencies and coupling strengths achievable in Rydberg atom tweezer arrays [6,40,42]. Finally, we note that the timescales associated with the effective interaction dynamics, $\tau_3 = \hbar/V_3$, are < 50 μs in a wide region of the parameter space [i.e., the nonhatched area in Fig. 2(b)] and are thus significantly shorter than the lifetime of the Rydberg states used in tailoring the MW-dressed potential of Fig. 2(a), which are of the order of hundreds of microseconds [50].

Phase diagram for a bipartite lattice.—We now focus on a system of atoms arranged on a bipartite lattice and investigate the effects of the interplay between (two-body) dipolar and effective (two- and three-body) interactions on its phase diagram. The simplest case of a square lattice is shown in Fig. 3(a). The different contributions to atom-atom interaction are listed in Figs. 3(a) and 3(c). Importantly, the lattice-dependent structure of H_{3B} in Eq. (6b) implies that effective two-body interactions are attractive while, on the contrary, three-body terms have a repulsive character. This feature is quite general and, e.g., in Ising spin models on nonbipartite lattices (triangular, kagome) it could be employed to implement frustrated interactions [15,19–21]. The study of such phenomena will constitute the focus of future investigations. Because of the competition between two- and three-body interactions, we expect that different phases emerge. To map out the phase diagram, we consider the classical limit (i.e., with vanishing Rabi frequency Ω) and determine its ground state through a classical Metropolis algorithm [62,63] by employing an annealing scheme [64].

Results are displayed in Figs. 4(a)–4(c). Here, we show the behavior in the $V_2 - V_3$ plane (with $V_1 > 0$ and $V_{3,x} = V_{3,y}$) of the average value of the Rydberg excitation

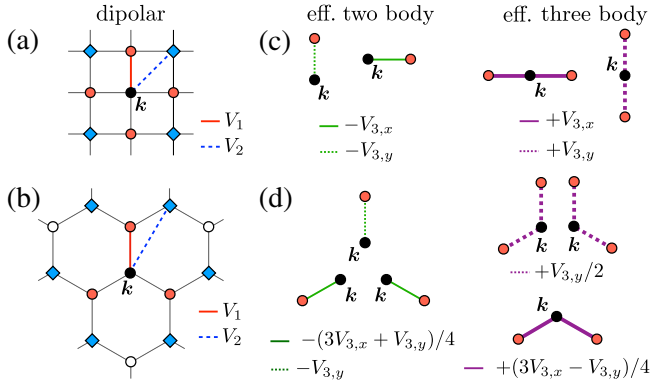

FIG. 3. Interaction terms in bipartite lattices. (a) Square and (b) honeycomb lattice with NNs (orange dots) and NNNs (blue squares) interacting through dipolar interactions (red solid and blue dashed lines, respectively). As a consequence of the phonon-mediated coupling, effective multibody interaction terms arise. Two-body (green, left) and three-body (purple, right) contributions along the horizontal (solid line) and vertical (dotted line) direction are shown, with their corresponding sign, in (c) and (d) for the square and honeycomb geometries, respectively. Note that, in the latter case, horizontal (solid line) terms contribute to both x and y directions, resulting in anisotropic interactions.

density $\langle n \rangle$ of the density of dimers $\langle n_{\mathrm{dim}} \rangle$ and of the density of trimers $\langle n_{\mathrm{trim}} \rangle$ [see Figs. 3(c) and 3(d)]. Beyond the trivial states with all excited and all deexcited atoms, four further phases emerge, see Fig. 4(d), which are (1) checkerboard phase, dominated by the repulsive contribution $\propto V_1$, (2) striped phase with a single three-atom stripe, dominated by NNN two-body (attractive) interaction $\propto V_2$, (3) frustrated striped phase with one missing line [here, the trimers occurring in (2) are melted due to the three-body repulsive contribution $\propto V_3$], and (4) four-excitation clustered phase, dominated by attractive two-body interactions $\propto V_3$. Concerning the latter, we note that the transition is not as sharp as the other ones. Indeed, as can be seen from the last panel of Fig. 4(d), the lattice is not entirely covered by four-particle clusters. This may suggest either that (4) is a liquid phase or that it represents a critical region. A full covering can be obtained for $V_2 > 0$, where attractive NNN interactions contribute to enhance the energy gain in forming clusters.

Interestingly, effective interactions due to spin-phonon coupling give rise to finite-size frustration phenomena even in a square lattice in the presence of isotropic dipolar interactions. This is manifest in the emergence of the different striped phases (2) and (3): see Fig. 4, which displays the case of a lattice with an even number of sites. On the contrary, if an odd number of sites is considered, only a single regular striped phase emerges in this region of the phase diagram. However, a frustrated phase forms inside phase (1) (see SM [50]).

In nonsquare lattices, the geometrical factors characterizing phonon-mediated interactions [see Eq. (9)] give rise

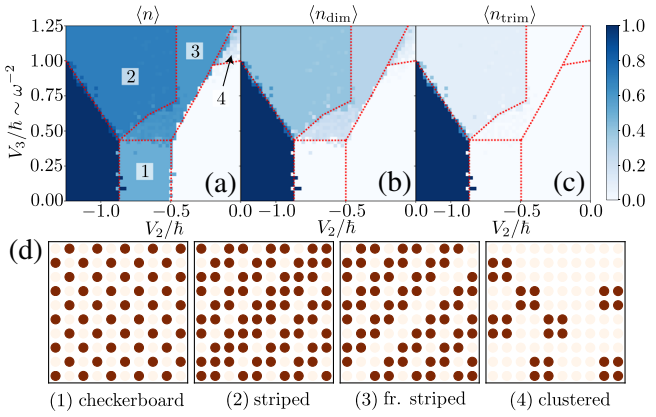

FIG. 4. Phase diagram (square lattice) as a function of $V_2/\hbar$ and $V_3/\hbar$. In (a) we show the average density of Rydberg excitations $\langle n\rangle$ as a function of $V_2/\hbar$ and $V_3/\hbar$ (units $2\pi\times$ MHz), with $V_{3,x}=V_{3,y}$, for a square lattice. Note that $V_{3,\mu}\sim\omega_\mu^{-2}$ and, therefore, it can be controlled by the confinement strength. (b),(c) Density of dimers $\langle n_{\mathrm{dim}}\rangle$ and trimers $\langle n_{\mathrm{trim}}\rangle$, respectively. Dashed red lines represent guides for the eye to distinguish between the different system phases. In (d) we show typical configurations in the different regions of the phase diagram. Dark (red) spots correspond to excited atoms. See text for details. In all panels, $L=10$, $V_1/\hbar=2\pi\times 0.2$ MHz, and $\Delta/\hbar=2\pi\times 1$ MHz.

to anisotropic two- and three-body contributions even if the original dipolar interactions between atoms are isotropic. This can be seen in Fig. 3(d), where the various interaction contributions arising in a honeycomb lattice are displayed. Here, though the phase diagram is similar to the one shown in Fig. 4, nontrivial and anisotropic system configurations emerge [50].

The various phases shown in Fig. 4 can be probed in state-of-the-art Rydberg simulators consisting of 2D defect-free arrays of optical tweezers [37]. Indeed, as shown in SM [50], a significant part of the phase diagram in Fig. 4 can be mapped out by employing trapping frequencies ω_μ ranging from a few tens to a few hundred kilohertz, while the required dipolar interaction couplings are of the order of a few megahertz. The desired many-body states can be prepared by real-time control of Rabi frequency and detuning via a generalization of the rapid adiabatic passage protocol proposed in Refs. [22,23] and demonstrated in Ref. [24]. The latter is perfectly compatible with the timescales associated with the effective interactions and, in turn, with the lifetime of the Rydberg states we considered.

Conclusions.—We have shown that electron-phonon interactions in Rydberg lattice quantum simulators permit the engineering of tunable multibody interactions. We have illustrated the underlying mechanism in bipartite lattices, discussing in particular the case of an isotropic square lattice, where we studied the phase diagram in the classical limit. Going beyond this limit and considering the impact of quantum fluctuations ($\Omega>0$) will be possible in Rydberg quantum simulator experiments. Many future directions of this work can be envisioned: In particular, we expect that, as a consequence of the lattice-dependent structure of the induced interactions, peculiar two- and three-body terms would arise in nonbipartite lattices (e.g., triangular, kagome), allowing for the investigation of frustrated magnetism in spin models with nontrivial multibody interactions. Furthermore, the mechanism leading from the spin-phonon coupling to effective many-body interactions can be generalized to different kinds of bare atom-atom potentials (e.g., exchange interactions, oscillating potentials) and may allow for engineering effective interactions with different structure and/or even n-body (with $n>3$) contributions.

The research leading to these results has received funding from the European Research Council under the European Union's Seventh Framework Programme (FP/2007-2013)/ERC Grant Agreement No. 335266 ("ESCQUMA"), the EPSRC Grant No. EP/M014266/1, the EPSRC Grant No. EP/R04340X/1 via the QuantERA project "ERyQSenS," and the Deutsche Forschungsgemeinschaft (DFG) within the SPP 1929 Giant interactions in Rydberg Systems (GiRyd). The simulations used resources provided by the University of Nottingham High-Performance Computing Service.

[1] T. F. Gallagher, *Rydberg Atoms* (Cambridge University Press, New York, 2005).
[2] M. Saffman, T. G. Walker, and K. Mølmer, Rev. Mod. Phys. **82**, 2313 (2010).
[3] R. Löw, H. Weimer, J. Nipper, J. B. Balewski, B. Butscher, H. P. Büchler, and T. Pfau, J. Phys. B **45**, 113001 (2012).
[4] M. Saffman, J. Phys. B **49**, 202001 (2016).
[5] C. Gross and I. Bloch, Science **357**, 995 (2017).
[6] H. Bernien, S. Schwartz, A. Keesling, H. Levine, A. Omran, H. Pichler, S. Choi, A. S. Zibrov, M. Endres, M. Greiner, V. Vuletić, and M. D. Lukin, Nature (London) **551**, 579 (2017).
[7] A. Browaeys, D. Barredo, and T. Lahaye, J. Phys. B **49**, 152001 (2016).
[8] Y. Y. Jau, A. M. Hankin, T. Keating, I. H. Deutsch, and G. W. Biedermann, Nat. Phys. **12**, 71 (2016).
[9] V. Lienhard, S. de Léséleuc, D. Barredo, T. Lahaye, A. Browaeys, M. Schuler, L.-P. Henry, and A. M. Läuchli, Phys. Rev. X **8**, 021070 (2018).
[10] A. Omran, H. Levine, A. Keesling, G. Semeghini, T. T. Wang, S. Ebadi, H. Bernien, A. S. Zibrov, H. Pichler, S. Choi, J. Cui, M. Rossignolo, P. Rembold, S. Montangero, T. Calarco, M. Endres, M. Greiner, V. Vuletić, and M. D. Lukin, Science **365**, 570 (2019).
[11] D. Ohl de Mello, D. Schäffner, J. Werkmann, T. Preuschoff, L. Kohfahl, M. Schlosser, and G. Birkl, Phys. Rev. Lett. **122**, 203601 (2019).
[12] D. Barredo, V. Lienhard, S. de Léséleuc, T. Lahaye, and A. Browaeys, Nature (London) **561**, 79 (2018).
[13] T. Vogt, M. Viteau, A. Chotia, J. Zhao, D. Comparat, and P. Pillet, Phys. Rev. Lett. **99**, 073002 (2007).
[14] T. Pohl, H. Sadeghpour, and P. Schmelcher, Phys. Rep. **484**, 181 (2009).

[15] A. W. Glaetzle, M. Dalmonte, R. Nath, I. Rousochatzakis, R. Moessner, and P. Zoller, Phys. Rev. X **4**, 041037 (2014).
[16] R. M. W. van Bijnen and T. Pohl, Phys. Rev. Lett. **114**, 243002 (2015).
[17] A. W. Glaetzle, R. M. W. van Bijnen, P. Zoller, and W. Lechner, Nat. Commun. **8**, 15813 (2017).
[18] H. Weimer, M. Müller, I. Lesanovsky, P. Zoller, and H. P. Büchler, Nat. Phys. **6**, 382 (2010).
[19] L. Balents, Nature (London) **464**, 199 (2010).
[20] A. W. Glaetzle, M. Dalmonte, R. Nath, C. Gross, I. Bloch, and P. Zoller, Phys. Rev. Lett. **114**, 173002 (2015).
[21] S. Whitlock, A. W. Glaetzle, and P. Hannaford, J. Phys. B **50**, 074001 (2017).
[22] T. Pohl, E. Demler, and M. D. Lukin, Phys. Rev. Lett. **104**, 043002 (2010).
[23] J. Schachenmayer, I. Lesanovsky, A. Micheli, and A. J. Daley, New J. Phys. **12**, 103044 (2010).
[24] P. Schauß, J. Zeiher, T. Fukuhara, S. Hild, M. Cheneau, T. Macrì, T. Pohl, I. Bloch, and C. Gross, Science **347**, 1455 (2015).
[25] J. K. Pachos and M. B. Plenio, Phys. Rev. Lett. **93**, 056402 (2004).
[26] H. P. Büchler, A. Micheli, and P. Zoller, Nat. Phys. **3**, 726 (2007).
[27] K. P. Schmidt, J. Dorier, and A. M. Läuchli, Phys. Rev. Lett. **101**, 150405 (2008).
[28] B. Capogrosso-Sansone, S. Wessel, H. P. Büchler, P. Zoller, and G. Pupillo, Phys. Rev. B **79**, 020503(R) (2009).
[29] L. Bonnes, H. Büchler, and S. Wessel, New J. Phys. **12**, 053027 (2010).
[30] G. Moore and N. Read, Nucl. Phys. **B360**, 362 (1991).
[31] A. Kitaev, Ann. Phys. (Amsterdam) **321**, 2 (2006).
[32] R. Moessner and S. L. Sondhi, Phys. Rev. Lett. **86**, 1881 (2001).
[33] G. Misguich, D. Serban, and V. Pasquier, Phys. Rev. Lett. **89**, 137202 (2002).
[34] A. M. Kaufman, B. J. Lester, and C. A. Regal, Phys. Rev. X **2**, 041014 (2012).
[35] F. Nogrette, H. Labuhn, S. Ravets, D. Barredo, L. Béguin, A. Vernier, T. Lahaye, and A. Browaeys, Phys. Rev. X **4**, 021034 (2014).
[36] H. Labuhn, S. Ravets, D. Barredo, L. Béguin, F. Nogrette, T. Lahaye, and A. Browaeys, Phys. Rev. A **90**, 023415 (2014).
[37] D. Barredo, S. de Léséleuc, V. Lienhard, T. Lahaye, and A. Browaeys, Science **354**, 1021 (2016).
[38] H. Labuhn, D. Barredo, S. Ravets, S. de Léséleuc, T. Macrì, T. Lahaye, and A. Browaeys, Nature (London) **534**, 667 (2016).
[39] M. Endres, H. Bernien, A. Keesling, H. Levine, E. R. Anschuetz, A. Krajenbrink, C. Senko, V. Vuletic, M. Greiner, and M. D. Lukin, Science **354**, 1024 (2016).
[40] M. Marcuzzi, J. Minář, D. Barredo, S. de Léséleuc, H. Labuhn, T. Lahaye, A. Browaeys, E. Levi, and I. Lesanovsky, Phys. Rev. Lett. **118**, 063606 (2017).
[41] A. Cooper, J. P. Covey, I. S. Madjarov, S. G. Porsev, M. S. Safronova, and M. Endres, Phys. Rev. X **8**, 041055 (2018).
[42] H. Levine, A. Keesling, A. Omran, H. Bernien, S. Schwartz, A. S. Zibrov, M. Endres, M. Greiner, and V. Vuletić, and M. D. Lukin, Phys. Rev. Lett. **121**, 123603 (2018).
[43] S. Saskin, J. T. Wilson, B. Grinkemeyer, and J. D. Thompson, Phys. Rev. Lett. **122**, 143002 (2019).
[44] G. D. Mahan, *Many-Particle Physics* (Kluwer Academic/Plenum Publishers, New York, 2000).
[45] K. Yosida, *Theory of Magnetism* (Springer-Verlag, Heidelberg, 1996); W. Nolting and A. Ramakanth, *Quantum Theory of Magnetism* (Springer-Verlag, Heidelberg, 2009).
[46] M. A. Ruderman and C. Kittel, Phys. Rev. **96**, 99 (1954).
[47] P. W. Anderson, Phys. Rev. **79**, 350 (1950).
[48] I. Dzyaloshinsky, J. Phys. Chem. Solids **4**, 241 (1958); T. Moriya, Phys. Rev. **120**, 91 (1960).
[49] D. Barredo, V. Lienhard, P. Scholl, S. de Léséleuc, T. Boulier, A. Browaeys, and T. Lahaye, Phys. Rev. Lett. **124**, 023201 (2020).
[50] See Supplemental Material at http://link.aps.org/supplemental/10.1103/PhysRevLett.124.043402 for additional details about the microwave dressing scheme, the small displacement approximation, the polaron transformation, the validity regimes of the model, the preparation of the classical ground state, and the phase diagram for a honeycomb lattice, which includes Refs. [51–54].
[51] I. I. Beterov, I. I. Ryabtsev, D. B. Tretyakov, and V. M. Entin, Phys. Rev. A **79**, 052504 (2009).
[52] J. Johansson, P. Nation, and F. Nori, Comput. Phys. Commun. **183**, 1760 (2012).
[53] J. Johansson, P. Nation, and F. Nori, Comput. Phys. Commun. **184**, 1234 (2013).
[54] F. M. Gambetta, I. Lesanovsky, and W. Li, Phys. Rev. A **100**, 022513 (2019).
[55] D. Porras and J. I. Cirac, Phys. Rev. Lett. **92**, 207901 (2004).
[56] R. Blatt and C. F. Roos, Nat. Phys. **8**, 277 (2012).
[57] J. Vogel, W. Li, A. Mokhberi, I. Lesanovsky, and F. Schmidt-Kaler, Phys. Rev. Lett. **123**, 153603 (2019).
[58] X.-L. Deng, D. Porras, and J. I. Cirac, Phys. Rev. A **72**, 063407 (2005).
[59] J. D. Thompson, T. G. Tiecke, A. S. Zibrov, V. Vuletić, and M. D. Lukin, Phys. Rev. Lett. **110**, 133001 (2013).
[60] S. Sevinçli and T. Pohl, New J. Phys. **16**, 123036 (2014).
[61] M. Marcuzzi, E. Levi, W. Li, J. P. Garrahan, B. Olmos, and I. Lesanovsky, New J. Phys. **17**, 072003 (2015).
[62] M. E. J. Newman and G. T. Barkema, *Monte Carlo Methods in Statistical Physics* (Oxford University Press, New York, 1999).
[63] K. Binder and D. W. Heermann, *Monte Carlo Simulation in Statistical Physics* (Springer-Verlag, Berlin Heidelberg, 2010).
[64] H. Gould, J. Tobochnik, and W. Christian, *An Introduction to Computer Simulation Methods* (Addison-Wesley, San Francisco, 2007).